Title Page

Title: Connectivity profile predictive of effective deep brain stimulation in obsessive compulsive disorder
Short title: Connectivity of effective DBS for OCD

Authors: Juan Carlos Baldermann M.D. *[1], Corina Melzer M.Sc. [2], Alexandra Zapf M.Sc. [3], Sina Kohl Ph.D. [1], Lars Timmermann Prof. [4], Marc Tittgemeyer Ph.D. [2], Daniel Huys M.D. [1], Veerle Visser-Vandewalle Prof.[5], Andrea A. Kühn Prof. [6], Andreas Horn Ph.D.**[6] and Jens Kuhn Prof.**[1,7]

* Corresponding author
** Both authors contributed equally to the study

Affiliation: [1] Department of Psychiatry and Psychotherapy, University of Cologne, Medical faculty, Cologne, Germany.
[2] Max-Planck-Institute for Metabolism Research Cologne, Cologne, Germany.
[3] Department of Medical Psychology | Neuropsychology and Gender Studies & Center for Neuropsychological Diagnostics and Intervention (CeNDI), University Hospital Cologne, Cologne, Germany.
[4] Department of Neurology, University Hospital Giessen & Marburg, Marburg, Germany.
[5] Department of Stereotactic and Functional Neurosurgery, University of Cologne, Cologne, Germany.
[6] Department of Neurology, Movement Disorders and Neuromodulation Unit, Charité - University Medicine (CCM), Berlin, Germany.
[7] Johanniter Hospital Oberhausen, Department of Psychiatry and Psychotherapy, Oberhausen, Germany

Corresponding Author: Juan Carlos Baldermann
Department of Psychiatry and Psychotherapy, University of Cologne, Medical faculty, Cologne, Germany, Kerpener Strasse 62, 50937 Cologne, Germany
Phone: + 49 (0) 221 478 4005; Fax: + 49 (0) 221 478 6030
Email: juan.baldermann@uk-koeln.de

Keywords: Obsessive-Compulsive Disorder (OCD); Diffusion-weighted magnetic resonance imaging (dMRI); Connectome; Lead-DBS; Deep brain stimulation (DBS); tractography
Wordcount: Number of words, abstract: 226; Number of words, article body: 3996; Number of Figures: 6; Number of Tables: 0; Supplemental data: 1

Abstract:

Background: Deep brain stimulation for obsessive-compulsive disorder is a rapidly developing treatment strategy for treatment-refractory patients. Both the exact target and impact on distributed brain networks remain a matter of debate. Here, we investigated which regions connected to stimulation sites contribute to clinical improvement effects and whether connectivity is able to predict outcomes.

Methods: We analyzed 22 patients (13 females) with treatment-refractory obsessive-compulsive disorder undergoing deep brain stimulation targeting the anterior limb of the internal capsule/nucleus accumbens. We calculated stimulation-dependent optimal connectivity separately for patient-specific connectivity data of 10 patients and for 12 additional patients using normative connectivity. Models of optimal connectivity were subsequently used to predict outcome in both an out-of-sample and in a leave-one-out cross-validation across the whole group.

Results: The resulting models successfully cross-predicted clinical outcomes of the respective other sample, and a leave-one-out cross-validation across the whole group further demonstrated robustness of our findings ($r = 0.630$; $p < 0.001$). Specifically, the degree of connectivity between stimulation sites and medial and lateral prefrontal cortices significantly predicted clinical improvement. Finally, we delineated a fronto-thalamic pathway that is crucial to be modulated for beneficial outcome.

Conclusion: Specific connectivity profiles, encompassing fronto-thalamic streamlines, can predict clinical outcome of deep brain stimulation for obsessive-compulsive disorder. After further validation, our findings may be used to guide both deep brain stimulation targeting and programming and inform non-invasive neuromodulation targets for obsessive-compulsive disorder.

Introduction

Obsessive-compulsive disorder (OCD) is amongst the most common neuropsychiatric disorders with a lifetime prevalence of 2.3% (1). The involvement of altered cortico-striato-thalamo-cortical (CSTC) loops along with a fronto-striatal dysfunction is a generally accepted concept in the pathophysiology of OCD (2, 3). Despite increasing knowledge about network impairments, there is very limited information about modulating which networks may help to improve symptoms in OCD.

Deep brain stimulation (DBS) has been successfully employed to alleviate symptoms in severe treatment-resistant OCD (4). Based on the aforementioned fronto-striatal dysfunction model, the ventral striatum (VS) with the nucleus accumbens (NAC) and the nearby anterior limb of the internal capsule (ALIC), have become the most common targets (see (5) for a review). Response rates show a high variability and to date, reliable predictors for the intervention have not been identified (4). Although the exact mechanism of DBS for OCD remains vague, there is increasing evidence that the stimulation exerts both local and distributed effects on functional brain networks (6). A study based on 11 subjects found that DBS induced a reduction in functional connectivity between the NAC and both medial and lateral prefrontal cortices and that this effect correlated positively with outcome (7). Structural connectivity to the right MFG was also identified to be associated with a better clinical response in a sample of six patients, whereas connectivity to the orbitofrontal cortex (OFC) was associated with non-response (8). Of note, studies assessing networks associated with DBS for OCD reveal wide-spread prefrontal structures and are based on small sample sizes. The heterogeneity in identifying cortico-striatal pathways that carry out beneficial effects in neuromodulatory treatment for OCD is also reflected by the different cortical targets used for transcranial magnetic stimulation (TMS), which include the dorsolateral prefrontal cortex (DLPFC), supplementary motor area (SMA) and OFC (see (9) for meta-analysis and overview).

In summary, although it seems certain that DBS has effects on distributed brain networks, it remains highly unclear which networks are associated with clinical improvement. It is however vitally important to characterize such therapeutic networks as they may serve to guide targeting for both invasive and noninvasive brain stimulation (10). In Parkinson‘s Disease (PD), recently, a study defined connectivity profiles of effective DBS electrodes (11). Moreover, these profiles were able to robustly predict

treatment outcome across cohorts and DBS centers. With similar knowledge in OCD, current neuromodulative treatment could be improved and new stimulation protocols developed, thereby increasing effectivity and possibly reducing adverse events.

Here, we aimed at assessing stimulation-dependent connectivity profiles that are associated with and predictive of outcome in DBS for OCD. First, we hypothesized that beneficial effects of DBS are associated with stimulation of a prefronto-striatal networks. Second, we hypothesized that stimulation-dependent connectivity profiles would predict individual outcomes of DBS for OCD in out-of-sample data.

Methods and Materials

Subjects and clinical assessments

Twenty-two patients (thirteen females) were recruited from the outpatient clinic of the psychiatric department for obsessive-compulsive spectrum disorders at the University Hospital of Cologne. All patients were diagnosed with severe treatment-refractory OCD, qualifying them for DBS surgery. Definition of severity and treatment-refractoriness are given in the supplemental data. Included patients underwent DBS surgery to the ALIC/NAC, receiving 2 quadripolar DBS electrodes (models 3389 (n = 19) or 3387 (n = 3), Medtronic, Minneapolis, MN). Preoperative clinical assessments included demographic data and evaluation of symptom severity using the Y-BOCS. Final assessment of symptom severity took place 12 months (± 1 months) after surgery when stimulation settings remained stable. All subjects provided written informed consent and the study was approved by the Ethics committee of the University of Cologne.

Imaging acquisition and preprocessing

For each patient, structural high-resolution T1-weighted images were acquired on a 3.0-Tesla Philips Healthcare MRI-scanner (Philips Medical Systems, Hamburg, Germany) at the University Hospital of Cologne before surgery. Postoperative computer tomography (CT) was obtained for each patient after surgery to verify correct electrode placement. A subgroup of ten patients (eight females) received preoperative diffusion magnetic resonance imaging (dMRI) using echo planar imaging (TR 16800 ms; TE 82 ms; FOV 220mm; voxel-size 1.7 × 1.7 × 1.7 mm; 90 sampling directions; b-value 3000s/mm²)

on a 3.0-Tesla Siemens Magnetom PRISMA (Siemens Medical System, Erlangen, Germany). A detailed description of dMRI data analysis is given in the supplemental.

DBS Lead Localization and Volume of Tissue Activated Estimation

DBS electrodes were localized using Lead-DBS software (www.lead-dbs.org) as described elsewhere (11). Briefly, postoperative CT scans were linearly coregistered to preoperative MRI using Advanced Normalization Tools (12) (http://stnava.github.io/ANTs/). A subcortical refinement step was added to adjust for brain shift that may have occurred during surgery (*brainshift correction-module* in Lead-DBS). Images were then normalized into ICBM 2009b Nlin asymmetric space using the SyN approach implemented in Advanced Normalization Tools. An additional subcortical refinement step was applied to attain a most precise subcortical alignment between patient and template space. Results were visually reviewed to confirm accuracy. Volumes of tissue activated (VTA) were modelled following the approach described in (11). Briefly, the E-Field was estimated using a finite element method on a four-compartment mesh describing local grey and white matter, as well as electrode contact and insulating material (see Figure 1 for schematic display of methods and Figure 2 for visualization of individual electrode localization).

Connectivity Estimation

For the patient-specific connectivity, a dMRI diffusion scheme implemented in DSI-Studio was used analogue to the assessment of the normative group connectome (see below). Specifically, diffusion data were reconstructed using generalized q-sampling imaging (13) with a diffusion sampling length ratio of 1.25. The restricted diffusion was quantified using restricted diffusion processing (14). A deterministic fiber tracking algorithm (14) was used, the angular threshold was 60 degrees. The step size was 0.86 mm. The anisotropy threshold was determined automatically by DSI Studio. Tracks with length below 10 mm were discarded. A total of 200000 tracts were calculated per subject. The whole-brain fiber set was then normalized into standard-stereotactic space following the approach described in (15, 16) as implemented in Lead-DBS. For normative structural connectivity, a publicly available group connectome was used that is based on multishell diffusion-weighted and T2-weighted imaging data from

32 subjects of the Human Connectome Project at Massachusetts General Hospital (ida.loni.usc.edu/ (17)) as described elsewhere (15).

Creating and validating a data-driven profile of "optimal DBS connectivity"

A data-driven approach to identify networks correlating with the clinical outcome across the sample was applied that has been introduced in the context of PD before (11). Briefly, from the whole-brain connectome estimated for each subject (or the normative HCP connectome), fibers running through the VTA were selected and projected to the brain in a weighted fashion. Weighting was performed on a normalized version of the E-Field gradient strength estimated during VTA calculation. Thus, fibers running through VTA regions where the E-Field was high received a higher score than fibers in the peripheral zones of the VTA. Connectivity strength was then expressed as (weighted) numbers of fiber tracts between stimulation sites and each brain voxel. In a second step, across the group of patients, each voxel on the resulting connectivity maps is then correlated with clinical improvement on the YBOCS score using Spearman's rank correlation coefficients, leading to R-maps. High R-values on these maps identify regions to which strong connectivity is associated with good clinical outcome. As described before (11), since tractography maps are generally not normally distributed, they were transformed into a Gaussian distribution following the approach of van Albada (18) and lightly smoothed before calculating the R-maps across the group. Due to the unnormal distribution of dMRI data, displays of cortical R-maps were restricted to positive correlations with outcome. A further subcortical tract-based analysis was performed to show fibertracts associated with negative outcome as described below.

Crucially, the R-map may be seen as a model for "optimal" connectivity from the DBS electrode to the rest of the brain, denoting high values for "good" regions (i.e. regions a connectivity to which is associated with good outcome) and low values for the opposite. To be able to make true predictions on a subset of our cohort, the approach (R-map calculation) was performed separately on the 10 patients with patient-specific dMRI available and the 12 patients for which the high definition HCP normative connectome was used as in prior work (11, 15, 19, 20). The resulting $R\text{-map}_{10}$ and $R\text{-map}_{12}$ was thus created on ~half of the cohort using either patient-specific connectivity data or normative connectivity data. To test its validity, the $R\text{-map}_{10}$ was used to cross-predict outcome of the remaining 12 patients with normative connectivity data and vice versa. To do so, similarity between individual connectivity

profiles in one sample and the respective R-map of the other sample was assessed by calculating Fisher z-transformed spatial Spearman correlations fitted to the empirical outcomes using a general linear model (11). This analysis shows how similar each VTAs connectivity profile within one sample is to the data-driven "optimal" connectivity profile of the other sample (defined by the R-map$_{10}$ and R-map$_{12}$) and demonstrates the predictive power of the R-map for out-of-sample data.

After this analysis, an additional R-map$_{22}$ was calculated across the whole group of subjects (with normative connectivity data) to estimate a final optimal connectivity profile informed by as many patients as possible. To validate this map, a leave-one-out cross-validation was applied, where in each step, one patient was taken out of the model and the empirical outcome was correlated with the predicted outcome derived from the remaining sample.

To further explore whether connectivity to specific cortical regions would be able to explain clinical improvement, we added a region of interest (ROI) analysis. This investigated the explanatory value of connectivity estimates from stimulation sites to specific ROI using the same normative connectivity analysis as on the R-map$_{22}$. ROIs were chosen from prior literature (7, 8) informed hypotheses, indicating that effective DBS is associated with involvement of the right MFG and left ACC. Thus, connectivity between each pair of VTA and right MFG and left ACC (derived from the automated anatomical labeling (AAL) atlas (21)) was correlated with clinical outcome using Spearman correlation. Finally, to extract subcortical streamlines predictive of outcome, fibertracts connected to VTAs across the group of patients were isolated from the normative connectome and a two-sample t-test was fitted for each tract between the Y-BOCS improvement scores corresponding to connected vs. unconnected VTAs. Fibers were then colored by t-values. For the latter analysis, we added a supplementary analysis of fibertracts associated with improvement of depressive symptoms as assessed by the Beck Depression Inventory (22) (see supplemental for further description). Ultimately, we verified the fibertract predictive of positive outcome in the YBOCS in a focal VTA-based analysis (see supplemental for further description).

Results

The overall sample included 22 patients (13 females, age 41.7 ± 12.3 years). Mean Y-BOCS before surgery was 31.3 ± 4.3. After 12 months, YBOCS scores decreased significantly by a mean of 30.4 ± 20.1 % ($p < 0.001$). There was no significant correlation between age at surgery ($r = 0.127$; $p = 0.574$) or preoperative baseline symptom severity ($r = -0.152$; $p = 0.499$) with clinical outcome.

DBS connectivity analysis

In the data-driven analysis, resulting maps denoted correlation coefficients between connectivity and clinical outcome across the group (R-maps). Such a map was calculated on two independent subsets of patients using patient-specific dMRI data ($n = 10$; R-map_{10}) and normative connectivity data ($n = 12$; R-map_{12}) and used to cross-predict outcome in the respectively remaining patients. Based on the R-map_{10} we were able to significantly predict outcomes of the normative connectivity sample ($r = 0.545$; $p = 0.024$). Inversely, we were able to significantly predict outcomes of patient-specific connectivity profiles using the normative R-map_{12} model ($r = 0.685$; $p = 0.011$) (Figure 3).

To define a final model of "optimal connectivity" informed by as many patients as possible, the same analysis was repeated across the full cohort (all using normative data; R-map_{22}; figure 4). Similarly, to the cohort-specific maps, a positive correlation between connectivity and clinical outcome resulted for areas involving the medial prefrontal cortex as well as the bilateral lateral prefrontal cortex. Verifying the validity of the model, individual outcomes were significantly predicted in a leave-on-out cross-validation ($r = 0.630$), $p < 0.001$).

A ROI-analysis of normative connectome data of the whole sample revealed, congruent to the R-map_{22}, significant correlations between clinical improvement and connectivity to the right MFG ($r = 0.602$; $p = 0.002$) (Figure 5). Connectivity to left ACC did not show a significant relationship with outcome ($r = 0.001$; $p = 0.996$).

In a final step, fibers predictive of effective DBS connected to VTAs across the whole sample were visualized in a color-coded fashion (Figure 6). This analysis highlighted a clear-cut fibertract within the ventral ALIC that passes by the ventral striatum, bordering the bed nucleus of the stria terminalis (BNST) and connects middle prefrontal cortex with the thalamus. Fibers associated with negative outcome encompassed streamlines to medial forebrain bundle (MFB), the posterior limb of the anterior commissure (AC) and fibers within the inferior lateral fascicle (ILF). In the VTA-based

analysis, the specific fiber bundle within the ALIC was confirmed, showing that VTAs reaching outlined white matter areas apical and posterior of the NAC displayed the highest mean improvement rates (sFigure 1).

A secondary analysis revealed that fibers encompassing the cingulum, ventromedial prefrontal cortex and the fornix were associated with improvement of depressive scores (sFigure 2). Of note, this additional analysis has to be interpret with caution as the intervention was not intended to improve depressive symptoms and was only performed in 17 patients with depression scores available.

Discussion

Based on our results, we were able to characterize networks that are associated with and predict reduction of symptoms of severe OCD by ALIC/NAC neuromodulation. We validated the applicability of normative connectome data by significantly cross-predicting outcome of DBS for OCD in two independent data sets consisting of patient-specific and normative connectome data. Further, we calculated a model of optimal stimulation connectivity encompassing the lateral and medial prefrontal cortex that was able to significantly predict outcome in the overall sample. Within the prefrontal cortex, our analysis underlined the pivotal role of the right MFG for successful DBS. Finally, we delineated a tractographic target predictive of clinical outcome within the fronto-thalamic radiation.

Connectivity of effective neuromodulation for OCD

We identified a structural network model originating from the stimulation site using both patient-specific (R-map$_{10}$) and normative connectomes (R-map$_{12}$) that is associated with symptom improvement after one year of DBS to the ALIC/NAC. Of note, with these models of effective stimulation we were able to cross-predict outcome in two independent samples based on both patient-specific and normative connectomes. Both networks of beneficial response revealed connectivity to the medial and lateral prefrontal cortex. In a subsequent analysis, we pooled patients to compute a more powered model of effective DBS. The resulting R-map$_{22}$ showed a positive correlation between connectivity to bilateral dorsolateral prefrontal cortices and the medial prefrontal wall including the cingulate cortex.

This data-driven approach was complemented with a ROI based approach. Specifically, we wanted to show that connectivity between stimulation sites and literature defined cortical regions could explain clinical improvement. This has the potential of using these cortical ROI in future analyses or studies to e.g. define optimal contacts, surgical targets or also DBS-unrelated analyses. Here, we found a significant positive correlation of outcomes and connectivity to the right MFG. This finding is congruent to the, to our knowledge, only study assessing tractography from DBS stimulation sites in OCD patients, which found responders to be connected to the right MFG, though this study comprised only six patients (8). It is also in line with results of Figee et al. (7), who found that changes in functional connectivity between stimulation sites and right lateral prefrontal cortex after DBS of the NAC to be significantly correlated with improvement.

In a further analysis of subcortical pathways capable of predicting positive outcome, we identified a clear-cut fiber bundle that channels through the ventral ALIC, connects the middle prefrontal cortex with the thalamus. This tract was highly discriminative between electrodes that led to optimal vs. suboptimal outcomes. The resulting white matter bundle predictive of DBS outcome formed a bottleneck within the ALIC and traversed dorsally to the NAC. Thus, we conclude that the ALIC was a more effective target in our sample, a finding that was shown very recently in Sapap3 mutant mice, the currently predominant OCD animal model (23). This tract is also in line a study that successfully targeted the BNST with DBS (24) and highlights the importance of this structure for research on OCD (25). Very interestingly, the extracted fiber bundle bordered the BNST, entered the ventral part of the thalamus at the border of the anterior and inferior thalamic peduncle with fibers reaching the medial dorsal nucleus and nucleus subthalamicus (sFigure 3). Thus, this fiber bundle comprises different targets that have been successfully employed for DBS for OCD, suggesting that these different targets form a common network (24, 26, 27). While connectivity of VTAs with fronto-thalamic radiation was predictive of response to DBS for OCD, non-response was associated with more caudally located VTAs connected to the medial forebrain bundle and anterior commissure. The notion that the ideal target may be located further away from the currently employed electrode positioning is also supported by the clinical experience that stimulation amplitudes applied in patients with OCD (in our sample median of 4.7 V) tend to be higher than those applied in patients with PD or tremor. Hence, adjusting stimulation

parameters modulating as many as possible tracts that were associated with good and as few as possible associated with poor outcome may improve response and reduce side effects. Regarding our sample, results advise stimulation of more apical and dorsal contacts with the goal of modulating the fronto-thalamic radiation within the ALIC. Still, given the small sample size, it is difficult to extract clear clinical recommendations before prospective validation. It may however conceivable that implanted patients that did not respond to DBS may still profit after readjustment of stimulation parameters aiming at capturing the identified specific fiber bundle.

The connectomic approach for predicting DBS outcome for OCD

In our analysis, we were able to significantly predict outcomes of stimulation-dependent structural connectivity profiles using both a patient-specific and a normative model of effective connectivity across independent cohorts. Although this cross-validation has been performed in a small sample and has to be interpreted with caution, the same approach could explain 40% of the variance in the whole sample ($r = 0.63$; $n = 22$) in a leave-one-out design. The predictive character of this analysis is all the more of relevance, as to date there are no robust and conclusive predictors for outcomes of DBS for OCD and around 40% of patients do not respond to this invasive and costly procedure (4).

The predictive value of connectivity informed brain stimulation for DBS has already been shown for patients with PD (11). With our results, which comprises the largest OCD sample investigated with such an approach, we add evidence and advocate to investigate the clinical usefulness of such analysis. After careful further validation of our results, it could be worthwhile to determine a patient-specific surgical target based on connectomic analyses based on preoperative tractography. A similar approach is already practiced in specialized centers for the case of depression (29). Moreover, the technique may be used to guide DBS programming. Based on the patient-specific tractogram of novel patients, suitable stimulation contacts could be proposed by a computer model to facilitate this tedious trial-and-error process.

By validating the patient-specific connectivity models using a normative connectome we further highlight the utility of such publicly available data. This approach can be helpful in cases where dMRI is not available for a patient or if hyperkinetic disorders render it impossible to acquire a high quality dMRI scan due to motion artifacts. As mentioned in (11) , normative connectomes from healthy subjects

have the advantage of large subject numbers, excellent signal to noise ratio, and acquisition using specialized MRI hardware designed for connectivity imaging. Such normative connectome data have proven valuable in predicting stroke symptoms from patient-specific lesions (20, 30, 31) or treatment improvement after TMS (32). Another advantage of the normative data is the lack of vulnerability to the low test-retest reliability (33) in dMRI processing pipelines which may form an obstacle to compare results across centers. In contrast, patient-specific fibertracts may be advantageous for individual preoperative target selection, bearing in mind individual variances in white matter bundles in the ALIC (34). Our analysis shows that results derived from normative connectomes may be used to predict patients with individualized connectivity data in a split-half design. This does not mean that the information is interchangeable but indirectly validates the potential of normative data. The present study would be highly underpowered to estimate if normative or patient-specific connectivity is better suited to make accurate predictions. We emphasize that both approaches have their advantages and disadvantages for individual patients. Potentially, a combination of both approaches will be a future direction (34). More future work is needed to determine how to best combine the strengths of normative connectomes, patient-based connectomes, and connectivity data from individual patients. Of note, OCD specific alterations of white matter architecture does not necessarily influence the cross-validation of patient-specific and normative data, as our approach does not directly compare structural connectivity strength values but rather correlates clinical outcomes with connectivity profiles in each group, thereby blotting out evenly distributed OCD pathologies of quantitative structural connectivity.

A different approach beside the tractographic approach could be to focus at local effects, e.g. on subcortical nuclei, in a purely VTA or electrode placement based analysis. Ultimately, both approaches are linked to each other and should reveal complementary results due to the neuroanatomical implications. This is also supported by our supplemental VTA-based analysis which highlights a specific white matter area within the ALIC that matched the fiber bundle in the tractographic analysis.

In the present work, fibers of passage through the stimulation volume were selected and analyzed, a practice that was recently termed activation volume tractography (AVT; (35)). A more elaborate competing method, pathway-activation modeling (PAM) has been introduced in the same paper. This method exclusively considers known fibertracts and estimates activation of those tracts based on the

electrode location and stimulation parameters. This analysis is not prone to including false positive tracts (while potentially introducing false negatives). However, a direct transfer from subthalamic DBS to ALIC-DBS is not straight-forward given here, the tracts with pathophysiological roles have been much less studied as they have been in the subthalamic region for PD. Still, the potential danger of including false positive tracts is specifically relevant because a recent study concluded that the average tractography algorithm results more false positive than true positive tracts (36). However, we note that precisely in this open competition, the algorithm used in the present study achieved the highest "valid connection" score among 96 methods. This comparably good ratio of true and false positives could thus be seen as a "conservative" tractography algorithm that is suitable for clinical connectomics such as the present one.

Conclusion

In conclusion, we were able to identify a network that is associated with and predictive of beneficial effects in DBS for OCD. This network comprised both medial and lateral frontal cortices, in particular the right MFG, merging to an outlined (pre)fronto-thalamic fiber bundle that passes the striatum within the ventral ALIC. In our sample increased connectivity of stimulation sites to this fronto-striato-thalamic pathway predicted a large amount of variance in clinical symptom alleviation after one year. After further validation, these beneficial connectivity patterns may help to guide both stereotactic surgery and DBS programming, in the future. Furthermore, our results may have implications for both cortical and subcortical – and both invasive and noninvasive – neuromodulation protocols.

Acknowledgments

This work was supported by the German Research Foundation (Deutsche Forschungsgemeinschaft, KFO-219 Grant, KU2665/1-2 to JK, and KFO-247 to AAK). AH received funding from Berlin Institute of Health, Prof. Klaus Thiemann Foundation and Stiftung Charité. We thank Prof. Nieuwenhuys for his advisory help with neuroanatomical considerations.

Disclosures

JK has received financial support for Investigator initiated trials from Medtronic GmbH. The other authors declare no conflict of interest.

References

1. Ruscio AM, Stein DJ, Chiu WT, Kessler RC (2010): The epidemiology of obsessive-compulsive disorder in the National Comorbidity Survey Replication. *Mol Psychiatry*. 15: 53–63.

2. Ahmari SE, Spellman T, Douglass NL, Kheirbek MA, Simpson HB, Deisseroth K, *et al.* (2013): Repeated cortico-striatal stimulation generates persistent OCD-like behavior. *Science*. 340: 1234–9.

3. Abe Y, Sakai Y, Nishida S, Nakamae T, Yamada K, Fukui K, Narumoto J (2015): Hyper-influence of the orbitofrontal cortex over the ventral striatum in obsessive-compulsive disorder. *Eur Neuropsychopharmacol*. 25: 1898–1905.

4. Alonso P, Cuadras D, Gabri??ls L, Denys D, Goodman W, Greenberg BD, *et al.* (2015): Deep brain stimulation for obsessive-compulsive disorder: A meta-analysis of treatment outcome and predictors of response. *PLoS One*. 10. doi: 10.1371/journal.pone.0133591.

5. Kohl S, Schönherr DM, Luigjes J, Denys D, Mueller UJ, Lenartz D, *et al.* (2014): Deep brain stimulation for treatment-refractory obsessive compulsive disorder: a systematic review. *BMC Psychiatry*. 14: 214.

6. Bourne SK, Eckhardt CA, Sheth SA, Eskandar EN (2012): Mechanisms of deep brain stimulation for obsessive compulsive disorder: effects upon cells and circuits. *Front Integr Neurosci*. 6. doi: 10.3389/fnint.2012.00029.

7. Figee M, Luigjes J, Smolders R, Valencia-Alfonso CE, Van Wingen G, De Kwaasteniet B, *et al.* (2013): Deep brain stimulation restores frontostriatal network activity in obsessive-compulsive disorder. *Nat Neurosci*. 16: 386–387.

8. Hartmann CJ, Lujan JL, Chaturvedi A, Goodman WK, Okun MS, McIntyre CC, Haq IU (2016): Tractography activation patterns in dorsolateral prefrontal cortex suggest better clinical responses in OCD DBS. *Front Neurosci*. 9. doi: 10.3389/fnins.2015.00519.

9. Zhou D-D, Wang W, Wang G-M, Li D-Q, Kuang L (2017): An updated meta-analysis: Short-term therapeutic effects of repeated transcranial magnetic stimulation in treating obsessive-compulsive disorder. *J Affect Disord*. 215: 187–196.

10. Fox MD, Buckner RL, Liu H, Chakravarty MM, Lozano AM, Pascual-Leone A (2014): Resting-state networks link invasive and noninvasive brain stimulation across diverse psychiatric and neurological diseases. *Proc Natl Acad Sci*. 111: E4367–E4375.

11. Horn A, Reich M, Vorwerk J, Li N, Wenzel G, Fang Q, *et al.* (2017): Connectivity Predicts deep brain stimulation outcome in Parkinson disease. *Ann Neurol*. 82: 67–78.

12. Avants BB, Tustison N, Song G (2009): Advanced Normalization Tools (ANTS). *Insight J*. 1–35.

13. Yeh FC, Tseng WYI (2011): NTU-90: A high angular resolution brain atlas constructed by q-space diffeomorphic reconstruction. *Neuroimage*. 58: 91–99.

14. Yeh FC, Verstynen TD, Wang Y, Fernández-Miranda JC, Tseng WYI (2013): Deterministic diffusion fiber tracking improved by quantitative anisotropy. *PLoS One*. 8. doi: 10.1371/journal.pone.0080713.

15. Horn A, Neumann W-J, Degen K, Schneider G-H, Kühn AA (2017): Toward an electrophysiological "sweet spot" for deep brain stimulation in the subthalamic nucleus. *Hum Brain Mapp.* . doi: 10.1002/hbm.23594.

16. Horn A, Ostwald D, Reisert M, Blankenburg F (2014): The structural-functional connectome and the default mode network of the human brain. *Neuroimage*. 102: 142–151.

17. Setsompop K, Kimmlingen R, Eberlein E, Witzel T, Cohen-Adad J, McNab JA, *et al.* (2013): Pushing the limits of in vivo diffusion MRI for the Human Connectome Project. *Neuroimage*. 80: 220–233.

18. van Albada SJ, Robinson PA (2007): Transformation of arbitrary distributions to the normal distribution with application to EEG test-retest reliability. *J Neurosci Methods*. 161: 205–211.

19. Ewert S, Plettig P, Li N, Chakravarty MM, Collins DL, Herrington TM, *et al.* (2018): Toward defining deep brain stimulation targets in MNI space: A subcortical atlas based on multimodal MRI, histology and structural connectivity. *Neuroimage*. 170.

20. Darby RR, Horn A, Cushman F, Fox MD (2017): Lesion network localization of criminal behavior. *Proc Natl Acad Sci*. 201706587.

21. Tzourio-Mazoyer N, Landeau B, Papathanassiou D, Crivello F, Etard O, Delcroix N, *et al.* (2002): Automated anatomical labeling of activations in SPM using a macroscopic anatomical parcellation of the MNI MRI single-subject brain. *Neuroimage*. 15: 273–289.

22. Hautzinger M, Bailer M, H. W&, Keller F (1994): Beck-Depressions-Inventar (BDI). Bearbeitung der deutschen Ausgabe. Testhandbuch. *Bern, Göttingen, Toronto, Seattle: Huber*. .

23. Pinhal CM, van den Boom BJG, Santana-Kragelund F, Fellinger L, Bech P, Hamelink R, *et al.* (2018): Differential effects of deep-brain stimulation of the internal capsule and the striatum on excessive grooming in Sapap3 mutant mice. *Biol Psychiatry*. . doi: 10.1016/j.biopsych.2018.05.011.

24. Luyten L, Hendrickx S, Raymaekers S, Gabriëls L, Nuttin B (2015): Electrical stimulation in the bed nucleus of the stria terminalis alleviates severe obsessive-compulsive disorder. *Mol Psychiatry*. 1–9.

25. Kohl S, Baldermann JC, Kuhn J (2016): The bed nucleus: A future hot spot in obsessive compulsive disorder research. *Mol Psychiatry*. 21. doi: 10.1038/mp.2016.54.

26. Jiménez F, Nicolini H, Lozano AM, Piedimonte F, Salín R, Velasco F (2013): Electrical stimulation of the inferior thalamic peduncle in the treatment of major depression and obsessive compulsive disorders. *World*

Neurosurg. 80. doi: 10.1016/j.wneu.2012.07.010.

27. Mallet L, Polosan M, Jaafari N, Baup N, Welter M-L, Fontaine D, *et al.* (2008): Subthalamic nucleus stimulation in severe obsessive-compulsive disorder. *N Engl J Med*. 359: 2121–2134.

28. Riva-Posse P, Choi KS, Holtzheimer PE, Crowell AL, Garlow SJ, Rajendra JK, *et al.* (2017): A connectomic approach for subcallosal cingulate deep brain stimulation surgery: prospective targeting in treatment-resistant depression. *Mol Psychiatry*. . doi: 10.1038/mp.2017.59.

29. Noecker AM, Choi KS, Riva-Posse P, Gross RE, Mayberg HS, McIntyre CC (2018): StimVision Software: Examples and Applications in Subcallosal Cingulate Deep Brain Stimulation for Depression. *Neuromodulation*. 21: 191–196.

30. Joutsa J, Horn A, Hsu J, Fox MD (2018): Localizing parkinsonism based on focal brain lesions. *Brain*. . doi: 10.1093/brain/awy161.

31. Joutsa J, Shih LC, Horn A, Reich MM, Wu O, Rost NS, Fox MD (2018): Identifying therapeutic targets from spontaneous beneficial brain lesions. *Ann Neurol*. . doi: 10.1002/ana.25285.

32. Whitwell JL, Shiung MM, Przybelski SA, Weigand SD, Knopman DS, Boeve BF, *et al.* (2008): MRI patterns of atrophy associated with progression to AD in amnestic mild cognitive impairment. *Neurology*. 70: 512–520.

33. Petersen M V., Lund TE, Sunde N, Frandsen J, Rosendal F, Juul N, Østergaard K (2017): Probabilistic versus deterministic tractography for delineation of the cortico-subthalamic hyperdirect pathway in patients with Parkinson disease selected for deep brain stimulation. *J Neurosurg*. 126: 1657–1668.

34. Nanda P, Banks GP, Pathak YJ, Sheth SA (2017): Connectivity-based parcellation of the anterior limb of the internal capsule. *Hum Brain Mapp*. 38: 6107–6117.

35. Gunalan K, Chaturvedi A, Howell B, Duchin Y, Lempka SF, Patriat R, *et al.* (2017): Creating and parameterizing patient-specific deep brain stimulation pathway-activation models using the hyperdirect pathway as an example. *PLoS One*. . doi: 10.1371/journal.pone.0176132.

36. Maier-Hein KH, Neher PF, Houde J-C, Côté M-A, Garyfallidis E, Zhong J, *et al.* (2017): The challenge of mapping the human connectome based on diffusion tractography. *Nat Commun*. 8: 1349.

Figures

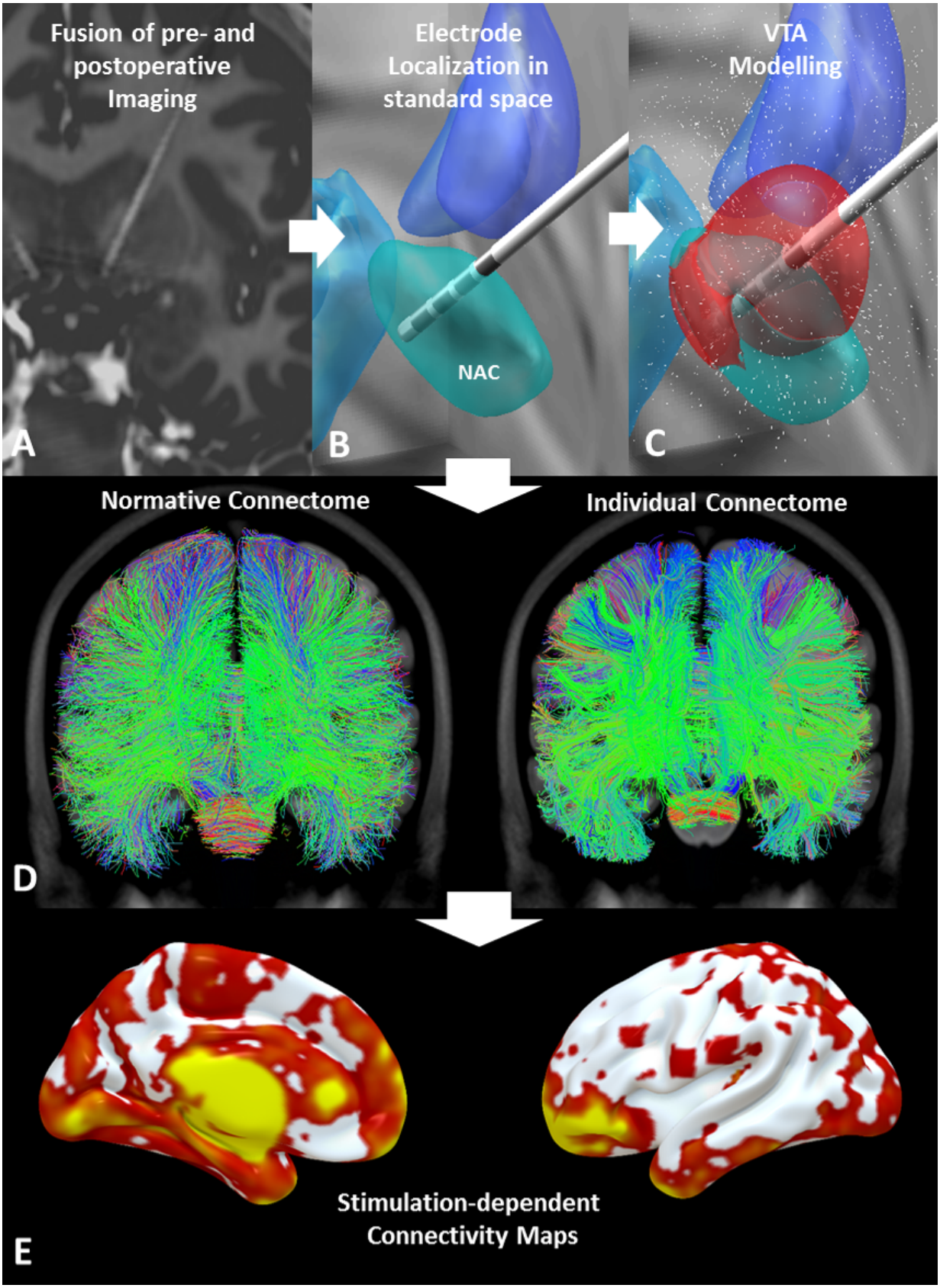

Figure 1: Schematic display of methods applied for identifying deep brain stimulation connectivity. Processing steps included fusion of pre-/postoperative imaging (A), localizing DBS leads in standard

space (B), modelling volumes of tissue activated (VTA) based on individually applied stimulation parameters (C), calculating both normative and (if available) individual structural (D) connectivity from the VTA to the whole brain, and isolating and weighting fibertracts passing VTA model, resulting in stimulation-dependent connectivity maps (E).

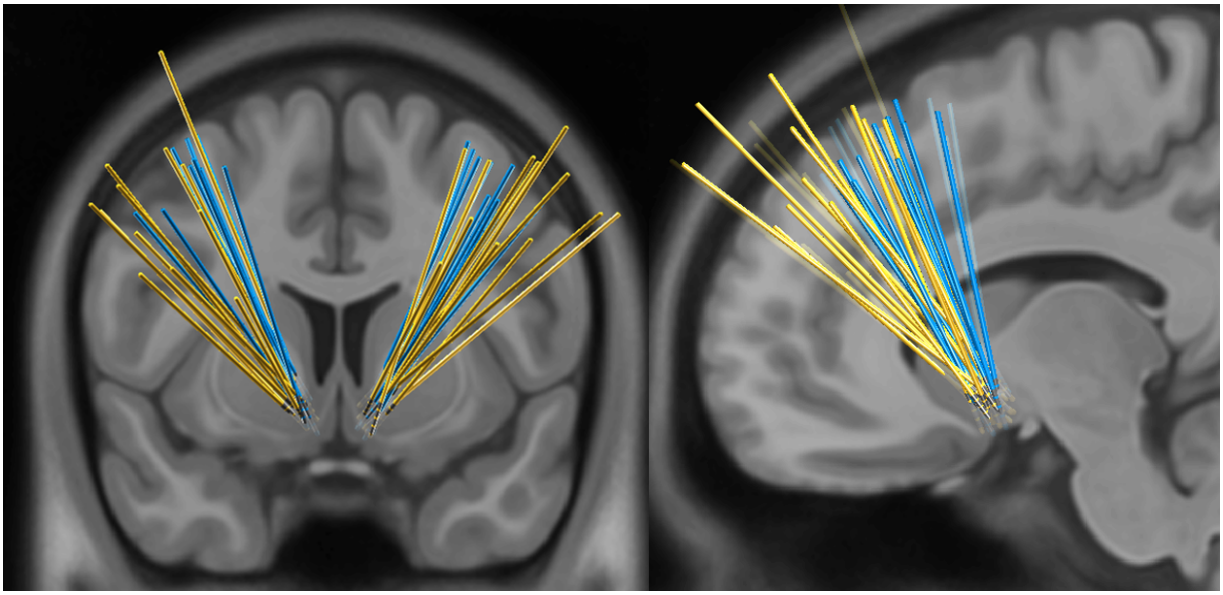

Figure 2: Localization of individual leads: All patients underwent DBS surgery to the anterior limb of the internal capsule with the tip of the electrodes located at the posterior border of the Nucleus Accumbens, receiving 2 quadripolar DBS electrodes. Blue leads represent patients were individual diffusion imaging was available (n = 10), yellow leads correspond to the remaining patients (n = 12).

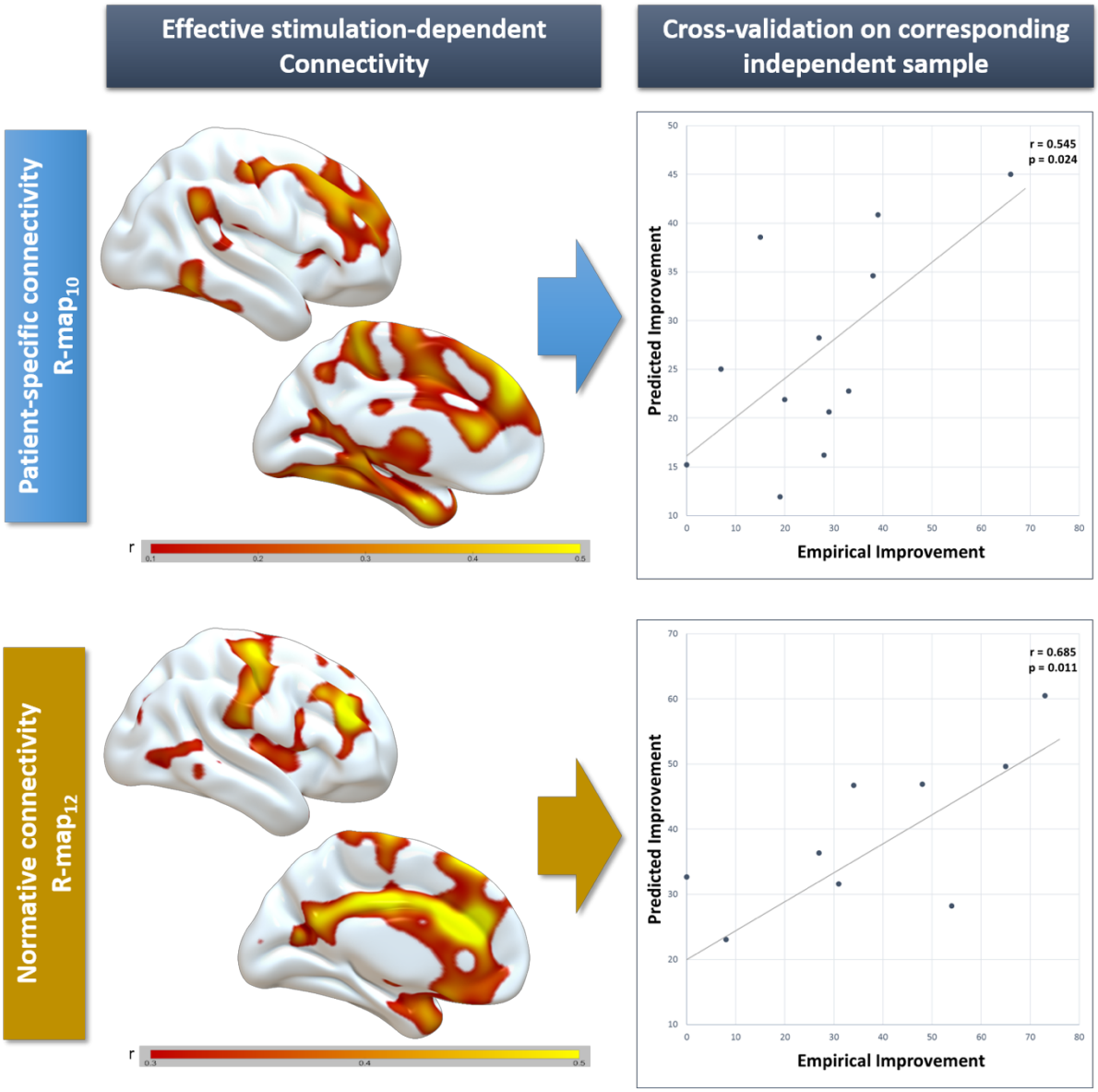

Figure 3: Maps of effective stimulation-dependent connectivity and clinical outcome derived from patient-specific (blue group, upper row, R-map$_{10}$, n=10) and normative connectomes (yellow group, bottom row, R-map$_{12}$, n=12) in two independent samples. R-values for connectivity to peak voxels were higher than displayed, since the maps were lightly smoothed for visualization (FWHM = isotropic 6 mm). To test validity, we successfully predicted outcome (indicated as % change in the Yale-Brown Obsessive Compulsive Scale) of the respective other sample using the R-map$_{10}$ model ($p = 0.024$) and the R-map$_{12}$ model ($p = 0.011$).

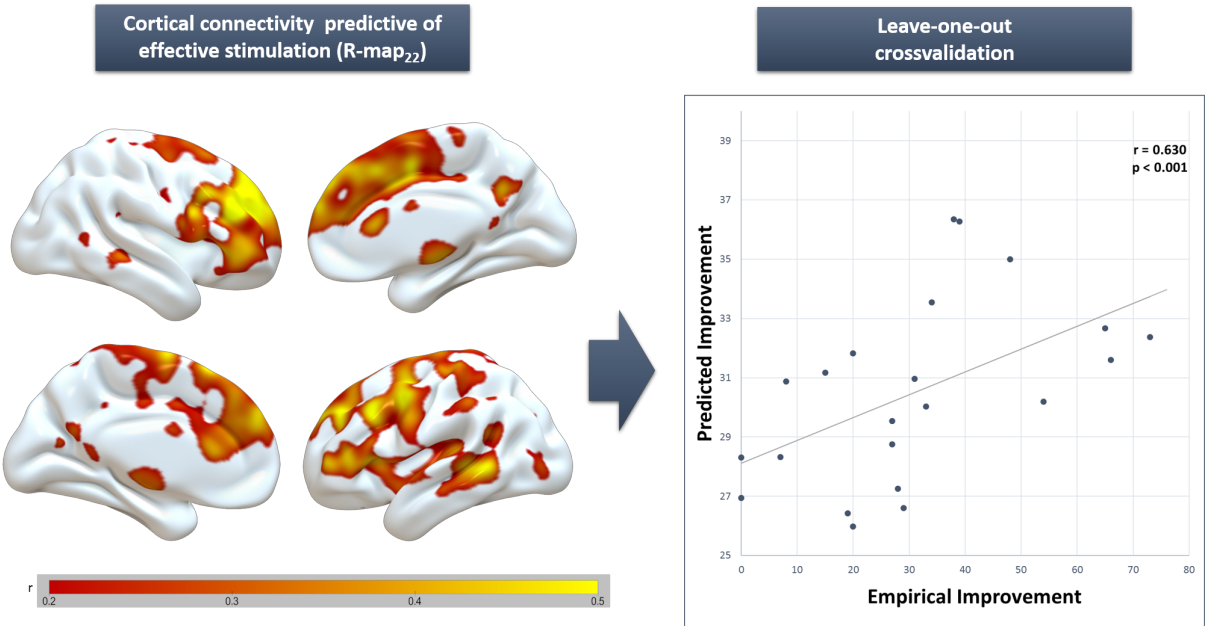

Figure 4: Model of stimulation-dependent connectivity and clinical outcome derived normative connectomes of the whole sample (R-Map$_{22}$, n = 22). To test validity of the resulting model of ideal connectivity, we successfully predicted outcomes of individual patients using a leave-one-out design (r = 0.630; p < 0.001), explaining ~40 % of the variance in clinical improvement (indicated as % change in the Yale-Brown Obsessive Compulsive Scale).

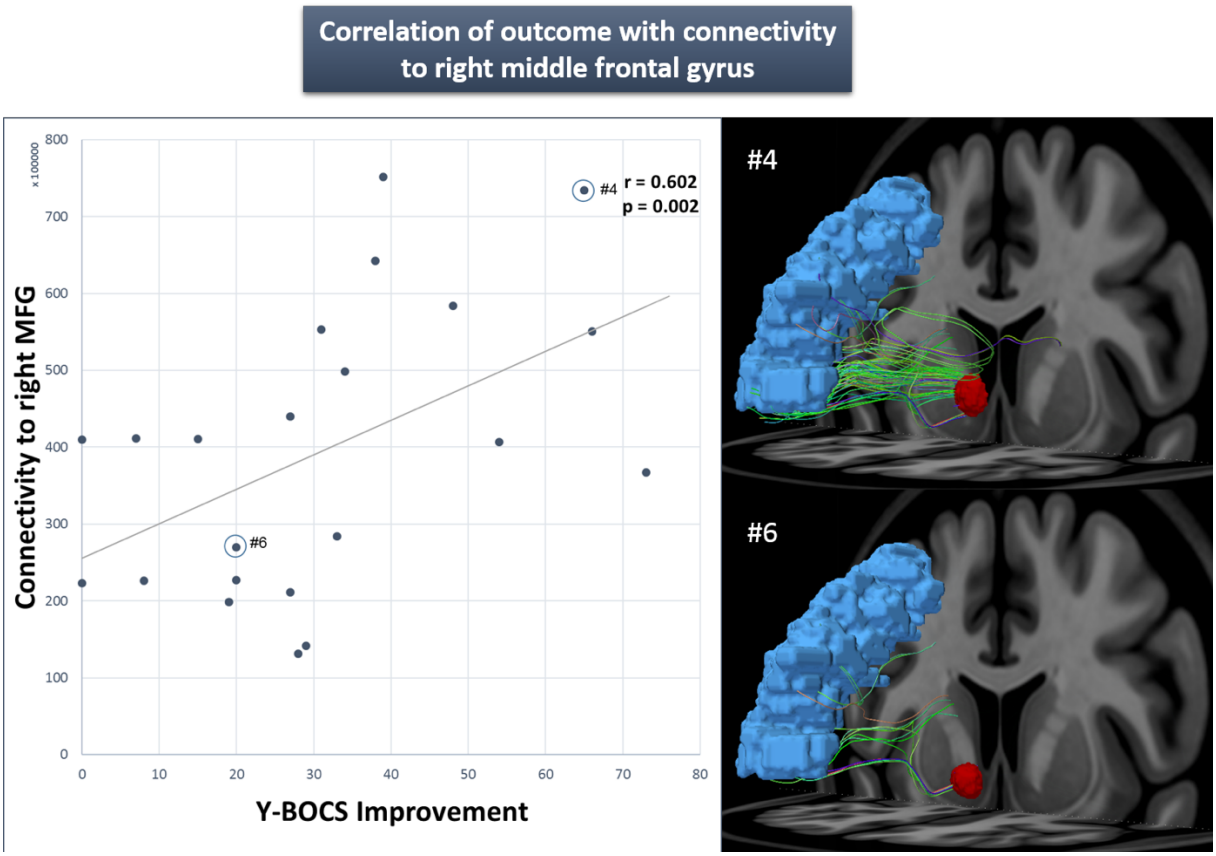

Figure 5: Correlation of outcome and connectivity to region of interest. Connectivity of stimulation sites to the right middle frontal gyrus (MFG) correlated significantly with the outcome of deep brain stimulation after one year (indicated as % change in the Yale-Brown Obsessive Compulsive Scale). On the right side, two exemplary patients are displayed. Patient #6, who did not respond sufficiently to the intervention and showed relatively sparse connectivity between stimulation site and MFG, whereas patient #4 exhibited enhanced connectivity to the caudal part of the MFG region, accompanied by a marked improvement in the Yale-Brown Obsessive Compulsive Scale (Y-BOCS).

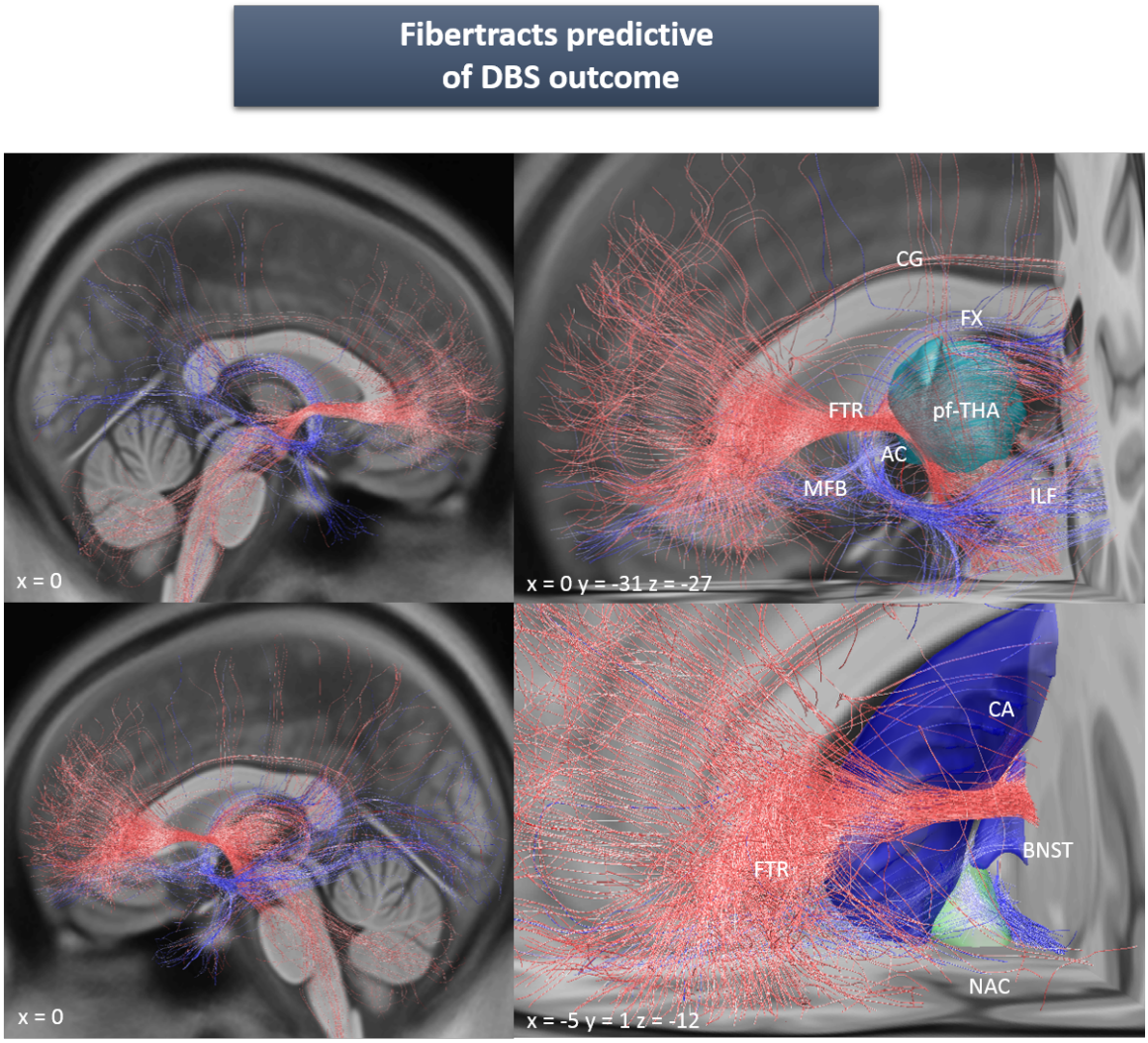

Figure 6: Fibertracts predictive of positive (red) or negative (blue) clinical outcome when connected to volumes of tissue activated (VTA) across the group of patients (n = 22). For each fibertract of the normative connectome, a two-sample t-test was fitted between the Y-BOCS improvements corresponding to connected vs. unconnected VTAs. Fibers were then colored by t-values. Left panels show a lateral view, right panels display a close-up view with labelling, highlighting a strong

association between connectivity with the anterior fronto-thalamic radiation (FTR) and clinical response. This effective fiber bundle borders the bed nucleus of the stria terminalis (BNST) and enters the ventral part of the thalamus (cyan) that is connected to the prefrontal cortex (pf-THA). Additionally, negative association with more ventrally situated VTAs connected to medial forebrain bundle (MFB) or anterior commissure (AC), whose posterior limb traverses to the temporal cortex, as well as inferior lateral fascicle (ILF) and Fornix (FX) becomes evident. (CG: Cingulum; CA: Nucleus Caudatus; NAC: Nucleus accumbens).

Supplemental

Supplemental methods

Subjects and clinical assessments

Severity was defined by a score of 25 or higher on the Yale-Brown Obsessive Compulsive Scale (Y-BOCS) (12) and a high impairment in functioning as indicated by a Global Assessment of Functioning (GAF) (13) score under 40. Treatment-resistance had to include at least one trial of cognitive behavioral therapy with exposure and response management over more than 45 sessions, at least two treatment trials with selective serotonin reuptake inhibitors (SSRI) over at least ten weeks in maximum dosage, one trial with clomipramine over ten weeks also in maximum dosage, and an augmentation approach with either antipsychotic medication, lithium, or buspirone.

Imaging acquisition and preprocessing

dMRI data was acquired for 90 gradient directions uniformly distributed on a sphere. This measurement was initialized with a volume without any diffusion-weighting (B=0) and then obtained in 10 blocks, each including one B0, followed by 9 diffusion-weighted volumes. At the end of this measure an additional B0 was acquired. This set of volumes was completely acquired with an anterior to posterior phase encoding direction. Additionally, a set of 8 non-diffusion-weighted MRI volumes was acquired with reverse phase encoding direction (post. to ant.), for later correction of susceptibility induced distortions. For estimating the distortion parameters, all non-diffusion-weighted volumes of the whole dMRI measurement (12 AP, 8 PA) were extracted and merged to perform FSL-Topup in FSL (version 5.0.8; http://fsl.fmrib.ox.ac.uk/fsl). The resulting parameters were then passed to FSL-eddy for applying distortion correction to the dMRI data, and correct for eddy currents and volume-wise motion.

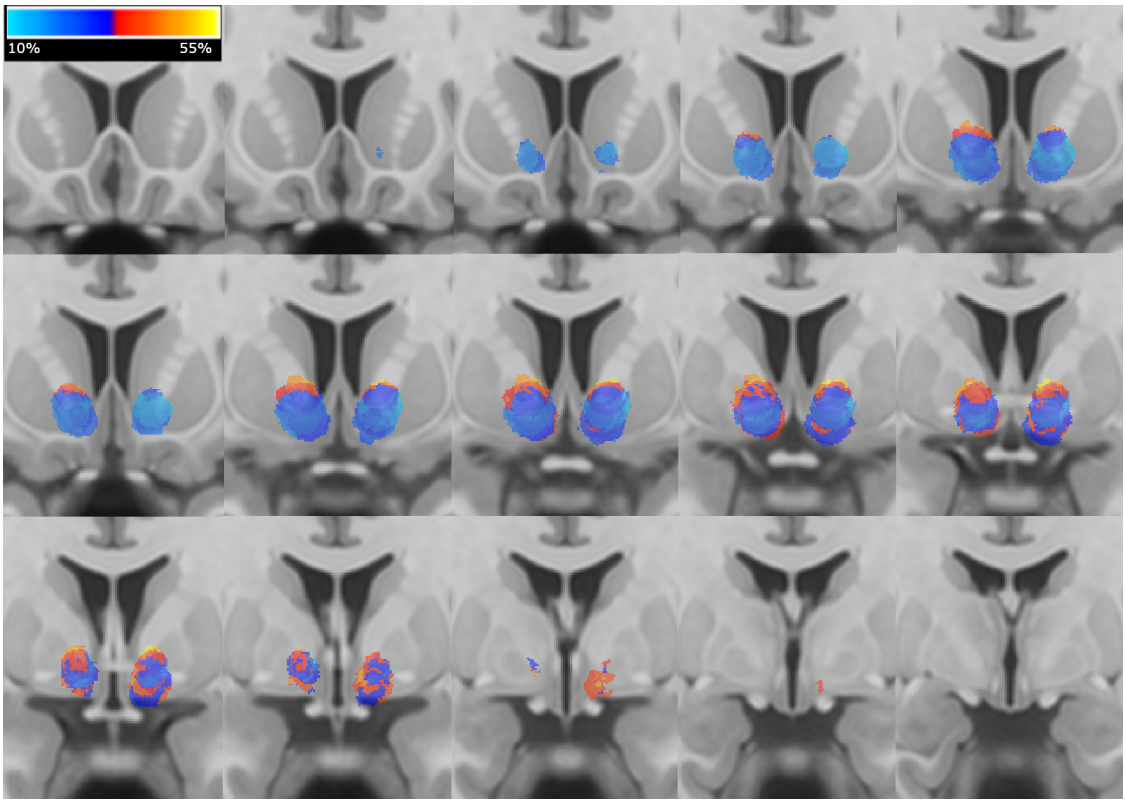

sFigure 1: VTA-based analysis. For this analysis, we overlapped individual VTAs and calculated for each voxel the mean percentage improvement rates of corresponding patients according to the YBOCS. To control for outliers, voxels that were covered by less than 20 % of patients were discarded. Best results were observed for VTAs located in a specific apical and posterior white matter area of the ALIC. This region corresponded to the fiber bundle predictive of positive outcome of DBS for OCD in the subcortical tractography analysis.

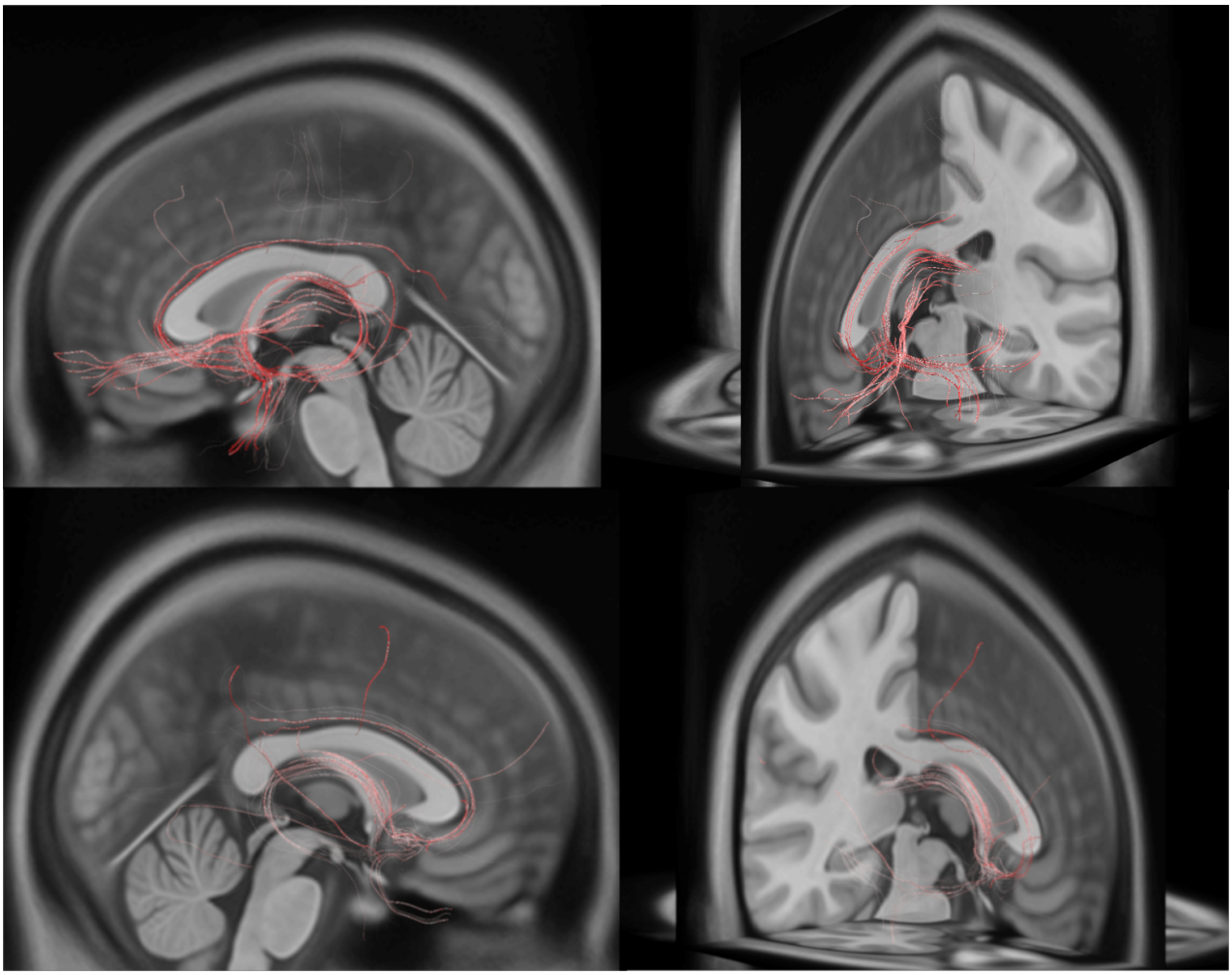

sFigure 2: Fibertracts associated with improvement of depressive Symptoms connected to volumes of tissue activated (VTA) across the group of patients with depression scores available (n = 17). For this additional analysis, we used absolute changes in the Beck Depression Inventory (BDI) from baseline to twelve months, because only a part of the patients had a clinically relevant depression at surgery. Mean preoperative scores (20.0 ± 10.0) indicated a moderate manifestation of depressive symptoms across the group that did not change significantly after twelve months (18.6 ± 12.4). Thus, percentage changes would have distorted the analysis significantly towards the less depressed patients. Antidepressant effects were found to be associated with fibers encompassing the cingulum and the fornix and partly fibers connecting the left ventromedial prefrontal cortex. Due to the methodological issues of this analysis, in particular the fact that the intervention was not intended to treat major depression, this results have to be interpret with all necessary caution.

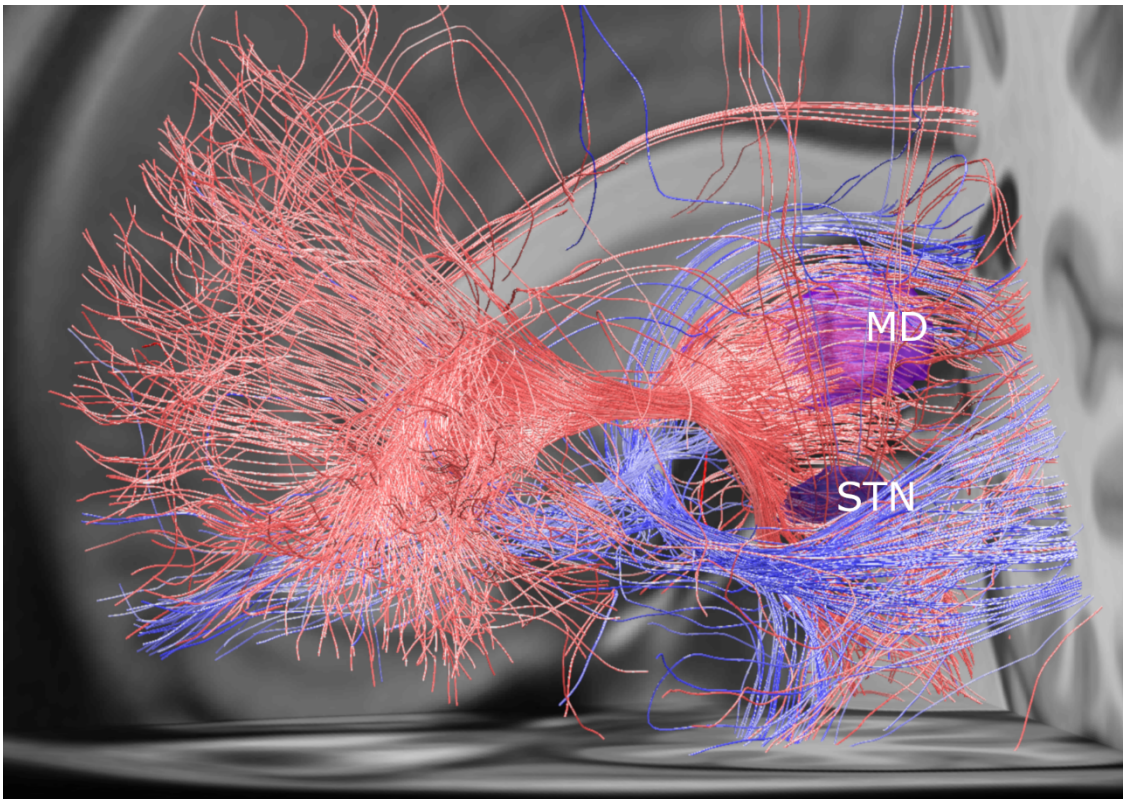

sFigure 3: Visualization of the identified fibertracts associated with outcome of DBS for OCD after twelve months and further nuclei relevant for OCD. The red fiber bundle predictive of a positive outcome carried fibertracts connecting the prefrontal fibers with the medial dorsal nucleus (MD) of the thalamus. Furthermore, we observed that parts of the specific fronto-thalamic fiber bundle descended directly ventrally of the STN, another successfully employed target for OCD.

CLUSTER	REGION	VOXEL	HEMISPHERE	X	Y	Z	R
1	Superior Medial Gyrus	116522	L	-5	48	42	0.67
	Middle Frontal Gyrus		L	-32	2	57	0.49
	Middle Frontal Gyrus		R	37	26	43	0.40
2	Superior Temporal Gyrus	12255	L	-63	-42	15	0.62
	Middle Temporal Gyrus		L	-66	-17	-15	0.47
3	Parahippocampal Gyrus	8533	R	20	-4	-27	0.50
4	Parahippocampal Gyrus	5566	L	-20	-4	-29	0.59
5	Inferior Temporal Gyrus	4234	R	50	-57	-21	0.41

sTable 1: Local maxima of cortical areas showing a positive correlation of connectivity with outcome of deep brain stimulation after one year according to the R-Map$_{10}$. Given are clusters with a R-Values ≥ 0.4 and a voxel extend ≥ 100. Coordinates are reported in Montreal Neurological Institute (MNI) space.

CLUSTER	REGION	VOXEL	HEMISPHERE	X	Y	Z	R
1	Middle Frontal Gyrus	190173	R	42	39	27	0.68
	Anterior Cingulate Cortex		L	-6	36	20	0.59
	Postcentral Gyrus		L	-58	-14	37	0.59
	Middle Frontal Gyrus		L	-25	-4	50	0.59
	Superior temporal Gyrus		L	-50	-32	12	0.59
	Anterior cingulate Cortex		R	7	42	16	0.57
	Precentral Gyrus		L	-32	-19	53	0.57
2	Parahippocampal Gyrus	1605	L	-16	-13	-22	0.45
3	Medial Temporal Pole	1196	L	-28	7	-30	0.42
4	Insula	604	L	-40	9	-11	0.46
5	Inferior Occipital Gyrus	365	L	-43	-87	-2	0.44
6	Superior Frontal Gyrus	320	R	16	40	54	0.45
7	Inferior Frontal gyrus	228	R	44	8	9	0.41
8	Insula	222	L	-31	19	9	0.42

sTable 2: Local maxima of cortical areas showing a positive correlation of connectivity with outcome of deep brain stimulation after one year according to the R-Map$_{12}$. Given are clusters with a R-Values ≥ 0.4 and a voxel extend ≥ 100. Coordinates are reported in Montreal Neurological Institute (MNI) space.

CLUSTER	REGION	VOXEL	HEMISPHERE	X	Y	Z	R
1	Middle Frontal Gyrus	10664	R	44	39	27	0.54
	Superior Frontal Gyrus		R	17	45	51	0.50
	Middle Frontal Gyrus		R	24	40	33	0.49
2	Middle Frontal Gyrus	4913	L	-29	2	55	0.51
	Precentral Gyrus		L	-40	2	42	0.47
	Precentral Gyrus		L	-47	4	47	0.47
3	Middle Frontal Gyrus	1452	L	-43	25	41	0.52
4	Middle Temporal Gyrus	1439	L	-60	-44	2	0.43
	Middle Temporal Gyrus		L	-52	-33	6	0.43
	Middle Temporal Gyrus		L	-53	-34	5	0.43
5	Middle Frontal Gyrus	1049	L	-22	42	35	0.48
6	Supplementary Motor Area	330	L	-7	24	62	0.48
7	Supplementary Motor Area	219	R	6	2	47	0.43
8	Middle frontal Gyrus	206	R	51	25	37	0.42
9	Supplementary motor area	100	L	9	22	46	0.41

sTable 3: Local maxima of cortical areas showing a positive correlation of connectivity with outcome of deep brain stimulation after one year according to the R-Map$_{22}$. Given are clusters with a R-Values ≥ 0.4 and a voxel extend ≥ 100. Coordinates are reported in Montreal Neurological Institute (MNI) space.